Mon. Not. R. Astron. Soc. **000**, 000–000 (0000) Printed 29 September 2014 (MN LATEX style file v2.2)

Wide-field adaptive optics performance in cosmological deep fields for multi-object spectroscopy with the European Extremely Large Telescope

A. G. Basden,[1⋆] C. J. Evans[2] and T. J. Morris[1]
[1] *Department of Physics, South Road, Durham, DH1 3LE, UK*
[2] *UKATC, Royal Observatory, Blackford Hill, Edinburgh, EH9 3HJ, UK*

arXiv:1409.7631v1 [astro-ph.IM] 26 Sep 2014

29 September 2014

ABSTRACT

A multi-object spectrograph on the forthcoming European Extremely Large Telescope will be required to operate with good sky coverage. Many of the interesting deep cosmological fields were deliberately chosen to be free of bright foreground stars, and therefore are potentially challenging for adaptive optics (AO) systems. Here we investigate multi-object AO performance using sub-fields chosen at random from within the Great Observatories Origins Deep Survey (GOODS)-S field, which is the worst case scenario for five deep fields used extensively in studies of high-redshift galaxies. Our AO system model is based on that of the proposed MOSAIC instrument but our findings are equally applicable to plans for multi-object spectroscopy on any of the planned Extremely Large Telescopes. Potential guide stars within these sub-fields are identified and used for simulations of AO correction. We achieve ensquared energies within 75 mas of between 25-35% depending on the sub-field, which is sufficient to probe sub-kpc scales in high-redshift galaxies. We also investigate the effect of detector readout noise on AO system performance, and consider cases where natural guide stars are used for both high-order and tip-tilt-only AO correction. We also consider how performance scales with ensquared energy box size. In summary, the expected AO performance is sufficient for a MOSAIC-like instrument, even within deep fields characterised by a lack of bright foreground stars.

Key words: Instrumentation: adaptive optics, instrumentation: high angular resolution, Methods: numerical

1 INTRODUCTION

One of the primary scientific motivations for the forthcoming Extremely Large Telescopes (ELTs), which will have primary mirror diameters in excess of 20 m, is to understand the evolution of galaxies – from formation of the most distant systems known, seen only a few million years after the Big Bang, through to disentangling the structural components and histories of the nearby galaxies that we see today.

Many of the breakthroughs in galaxy studies over the past twenty years have been enabled by observations of selected "deep fields" on the sky. The core datasets for these efforts have been optical and near-infrared imaging from long integrations with the *Hubble Space Telescope (HST)* and ground-based observatories, complemented by a wealth of multi-wavelength information from facilities such as *Chandra*, *Spitzer*, *Herschel* and the Very Large Array (VLA).

Given the substantial observational investment in these fields, and the richness of the multi-wavelength data available, they will almost certainly be the target of future programmes with both the *James Webb Space Telescope* (JWST, Gardner et al. 2006) and the European ELT (E-ELT) (Spyromilio et al. 2008). Specifically, many of the sources known in these fields are sufficiently faint that they are beyond our current spectroscopic capabilities, and follow-up spectroscopy will require the improved sensitivities of these exciting new facilities.

One of the most important new techniques for studies of high-redshift galaxies over the past decade has been the development of integral-field spectrographs (IFSs) on 8-10 m class telescopes. These have enabled *spatially-resolved* studies of galaxies out to a redshift of $z \sim 3$ (see, e.g., the review by Glazebrook 2013). In particular, the use of adaptive optics (AO) with IFS instruments has provided unprecedented views of the substructure and physical properties of high-

⋆ E-mail: a.g.basden@durham.ac.uk (AGB)

© 0000 RAS

z galaxies (see, e.g., the comparisons of AO-corrected and seeing-limited observations from Newman et al. 2013).

However, at $z \gtrsim 1.5$ we are currently limited to spatially-resolved spectroscopy of only the most luminous and/or massive galaxies; to observe a representative sample of the galaxy population in the early Universe we require the spectroscopic sensitivity of the E-ELT. Moreover, to compile large samples (of thousands) of objects within a realistic observing time, we require the combination of multiple integral field units (IFUs) and a wide-field AO system.

The technical requirements for such observations, in particular the necessary AO performances, were presented by Puech et al. (2008, 2010). In brief, to probe scales of $\sim$1 kpc at high redshift (e.g., Bournaud et al. 2007) we require ensquared energies of 20 to 30% in $\sim$75 mas in the H-band. Coarser sampling of $\sim$100 to 150 mas (with comparable ensquared energy) is sufficient for the recovery of large-scale dynamics in the target galaxies. These requirements strongly influenced the conceptual design for the proposed EAGLE instrument (Cuby et al. 2010), and they are now shaping the design of the MOSAIC concept (Evans et al. 2014; Hammer et al. 2014) for a multi-object spectrograph (MOS) for the E-ELT. As noted above, many of the potential targets for MOS observations with any of the planned ELTs will likely be located in the existing extragalactic deep fields. To achieve the multi-object AO (MOAO) correction for an instrument such as MOSAIC we need natural guide stars (NGSs) within the patrol field of the instrument, but a key feature of the deep fields was that they were deliberately chosen to be free of relatively bright foreground stars (to avoid problems relating to saturation, diffraction, persistence, etc.). For example, the lack of suitable guide stars ($V < 14$) within a $2' \times 2'$ field for observations with the Multi-Conjugate Adaptive Optics Demonstrator (MAD, Marchetti et al. 2007), severely limited its use to observe cosmological deep fields.

In the following we therefore investigate whether we can obtain sufficient image quality for spatially-resolved spectroscopy of high-z galaxies in one of the most important extragalactic deep fields, the Great Observatories Origins Deep Survey (GOODS)-S field (Giavalisco et al. 2004). The GOODS-S field is one of five observed as part of the Cosmic Assembly Near-infrared Deep Extragalactic Legacy Survey (CANDELS; Grogin et al. 2011), providing unprecedented depth and wavelength coverage for such a large area of *HST* imaging. In addition to the rich photometric catalogues, there has been significant spectroscopic follow-up of galaxies in the GOODS-S field (e.g. Popesso et al. 2009), and this will be extended by the recently approved VANDELS ESO Public Spectroscopic Survey (PIs: R. McLure & L. Pentericci). Thus, in the coming years we will have considerable information in the GOODS-S region to select well-defined samples of target galaxies for spatially-resolved spectroscopy with the ELTs.

In addition to considering the GOODS-S field, we have performed a study of other fields including GOODS-N, UDS, EGS and COSMOS (Grogin et al. 2011). Within each of these fields, we have taken a random sample of ten 10 arcminute sub-fields and determined the number of stars within these fields with a r' magnitude of brighter than 16, and thus available for high order wavefront sensing (i.e. delivering more than a few photons per sub-aperture per frame). Table 1 shows the number of suitable NGSs within these sub-fields; the GOODS-S field provides the fewest guide stars within its sub-fields. We have therefore chosen these sub-fields for further study as the pessimistic case: our results are equally applicable for the other fields.

Table 1. NGS availability within ten random 10 arcminute sub-fields from within the given cosmological deep fields. The numbers presented are the number of sub-fields containing only N natural guide stars with $r' < 16$ mag.

Field	Sub-fields containing only N guide stars								
$N=$	2	3	4	5	6	7	8	9	>9
GOODS-S	1	2	2	4	1	0	0	0	0
GOODS-N	0	1	2	1	2	2	1	1	0
UDS	0	0	0	0	0	2	3	3	2
EGS	0	1	0	0	2	1	2	1	3
COSMOS	0	0	0	0	0	0	0	0	10

The NFIRAOS system on the Thirty Metre Telescope (TMT) has a science goal of 50% sky coverage, and is expected to deliver AO correction over most of the observable sky for 50% of fields (Andersen et al. 2011). The increased light collecting area of the E-ELT will further improve field observability. Since the GOODS-S field is looking directly out of the Milky Way galaxy, it is a pessimistic case. Indeed, a statistical approach to sky coverage for the E-ELT by European Southern Observatory (ESO) (Calamida 2009) found that, in a typical field at the latitude of the GOODS-S field, we would expect more guide stars than we find in this field (it is pessimistic), and that even at the Galactic pole we would expect at least a couple of stars. Therefore we are confident that the fields under consideration here are relevant for the whole sky.

In §2, we introduce the NGS fields that we investigate, and provide details of the AO modelling that we perform. In §3 we discuss our results, and we conclude in §4.

2 MODELLING OF ELT ADAPTIVE OPTICS IN THE GOODS-S FIELD

Within the GOODS-S Deep + Wide + ERS survey region from CANDELS we generated ten random $10'$ diameter fields to investigate potential NGS asterisms. Using the data assembled for the fourth United States Naval Observatory CCD Astrograph Catalog (UCAC4, Zacharias et al. 2013), we recovered the positions and magnitudes of stars within each field (which are complete down to $R \sim 16$ mag), and used these as inputs to investigate the range of simulated AO performances. Specifically, we use the cross-matched Sloan r'-band magnitudes (in the AB system) from the American Association of Variable Star Observers (AAVSO) Photometric All-Sky Survey (APASS).

Fig. 1 shows the fields that we have investigated, giving the NGSs available within these fields and their corresponding r'-band magnitudes. For reference, we also show the notional laser guide star (LGS) positions. The field centres are given in Table 2, and the overlap of the fields is shown graphically in Fig. 2. A key point of this study is that of random field selection, and by estimating AO performance in randomly selected sub-fields, we are able to demonstrate the availability of suitable NGS targets over the whole of

Table 2. Central coordinates for the 10′ fields in which we have investigated the AO performances (J2000).

Asterism	RA / degrees	Dec / degrees
0	53.10850525	-27.71668243
1	53.16623306	-27.81152534
2	53.19574356	-27.77984810
3	53.14884949	-27.71123886
4	53.16050720	-27.84217262
5	53.10297775	-27.83361053
6	53.18798828	-27.80929756
7	53.14844513	-27.74827385
8	53.08246613	-27.86190033
9	53.16571426	-27.89375114

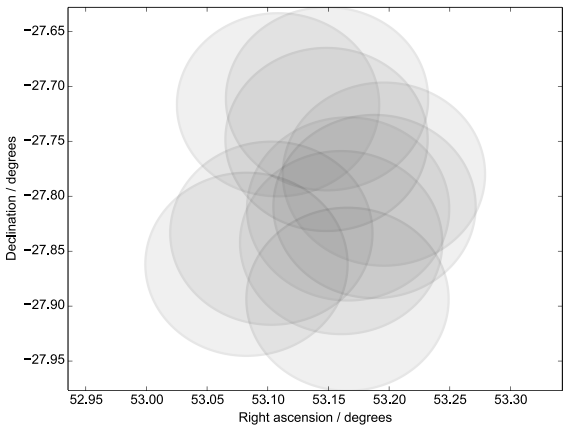

Figure 2. Positions of the ten random fields used to investigate potential NGS asterisms, within the GOODS-S field. The circles represent the 10 arcminute field-of-view of the telescope at each location.

the GOODS-S field. The alternative approach would be to determine all the NGS asterisms providing good AO performance within the GOODS-S field. However, it would then be necessary to accept that, if a scientific target lay just outside the corrected field of view, it would not be observable, or at least, the AO correction would be lower than required.

The faintest target that we consider has an r' magnitude of 16.3, which we translate to about three detected photons per sub-aperture per frame. We do not consider the use of any fainter targets as too few photons would be received. In the cases where NGSs are used for tip-tilt correction only, it would be possible to further reduce the source flux, though we do not investigate this here since the lack of high-order NGS information then leads to reduced AO performance (even if the tip-tilt stars are very bright).

2.1 Adaptive optics simulations

We use a Monte-Carlo simulation tool (Basden et al. 2007), the Durham AO simulation platform (DASP), to provide performance estimates for a MOAO-corrected MOS on the E-ELT, using the NGS asterisms defined in Fig. 1. The model has the same basic form as that used for performance modelling of the EAGLE concept (Basden et al. 2010), and previous analysis of E-ELT MOAO performances (Basden et al. 2013; Basden 2014). Although the exact details of the MOSAIC concept are still under study (e.g. number and final specification of science channels), our objective here was to investigate the broader aspects of a MOAO-corrected MOS, so we investigate a wide range of NGS magnitudes (§3), detector performances (§3.1), tip-tilt correction (§3.2), and spatial element size on-the-sky (§3.3). We note that the MOAO performance across the telescope field-of-view has been investigated previously (Basden et al. 2013), so here we provide on-axis performance estimates (at the centre of the LGS asterism) to simplify our results.

In summary, we use six sodium LGSs (589 nm wavelength) equally spaced around the edge of a 7.3 arcminute diameter circle (the widest LGS asterism that can be transported to the E-ELT focal plane), each with 74×74 sub-apertures and 16×16 pixels per sub-aperture. The telescope diameter is taken to be 38.5 m, and has a pupil function taken to match that of the multi-hexagon E-ELT. The secondary mirror obscuration is about 11 m in diameter, and the deformable mirror (DM) pitch is 52 cm. We have used a set of 35 layer atmospheric profiles, available on request from ESO. This profile is the result of years of data collection at the Paranal Observatory, and has an outer scale of $L_0 = 25$ m, and a Fried's parameter of $r_0 = 15.7$ cm defined at zenith. In the simulations presented here, we assume that observations are made at 30 degrees from zenith. We include the cone effect (due to the finite distance to the LGS spots) and spot elongation, assuming a sodium-layer profile with a Gaussian shape centred at 90 km with a 5 km full-width at half-maximum (FWHM). We use up to five NGSs, depending upon availability, and these are also sampled by 74×74 Shack-Hartmann wavefront sensor sub-apertures, which operate at the centre of the r'-band (625 nm). We do not take NGS chromatic effects into consideration. We include photon shot noise in our wavefront sensors (WFSs), and our default case includes no readout noise, though we investigate the effect on performance that this has in §3.1. In recent years, both electron multiplying CCD (EMCCD) and scientific CMOS (sCMOS) technologies have progressed significantly, and so it is likely that very low readout noise levels will be achievable within the time frame of ELT instrumentation. EMCCDs (Basden et al. 2003) routinely achieve 0.1 photo-electrons readout noise (with further reductions possible depending on their mode of operation), and sCMOS technology now achieves levels as low as 0.9 photo-electrons. For simplicity, we use a basic centre-of-gravity algorithm to estimate wavefront slope for both LGS and NGS WFSs, even though it has previously been shown that other algorithms can yield better performance, for example using correlation methods (Basden et al. 2014).

The E-ELT M4 deformable mirror is assumed to be conjugated to the ground-layer turbulence, and has 75×75 actuators. We investigate the H-band on-axis performance and use a MOAO DM with 75×75 actuators. Unless otherwise stated, our primary performance metric is the percentage of the point spread function (PSF) ensquared energy within 75 mas, chosen to match the scales of interest in high-z galaxies (Puech et al. 2008). A tomographic reconstruction of the atmospheric turbulence is performed using a minimum variance formulation, with phase covariance approximated by a Laplacian function. Noise covariance is assumed to be constant for each WFS, and dependent on

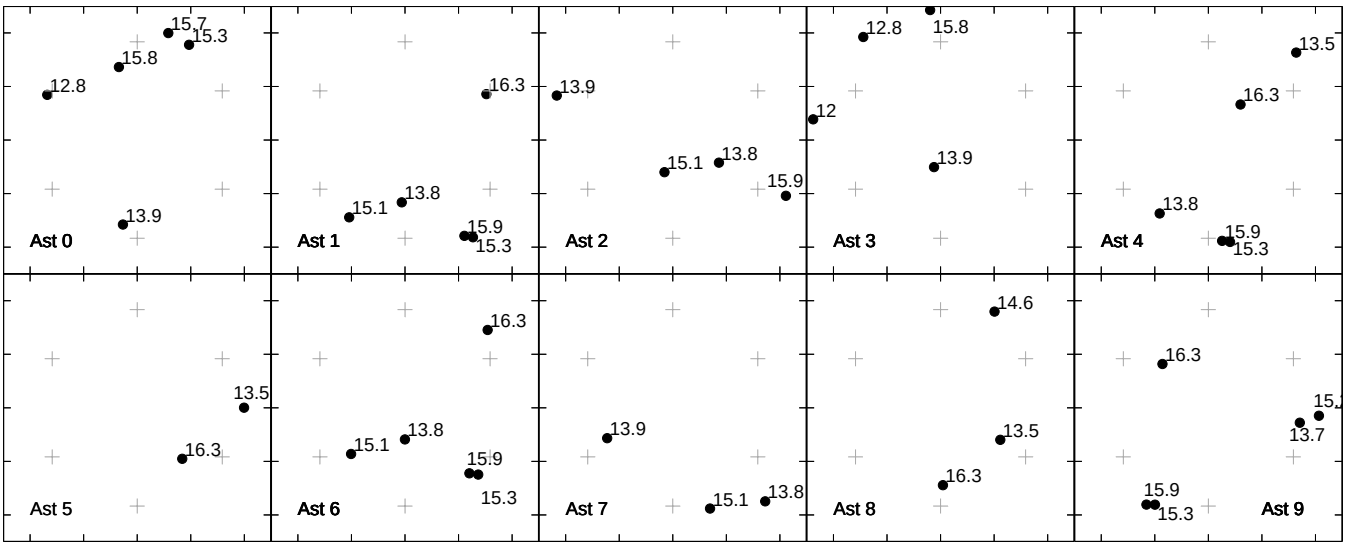

Figure 1. The ten NGS asterisms used to investigate potential AO performance in the GOODS-S field. Each sub-field is 10 arcminutes in diameter. The numbers within these figures provide the corresponding guide star r'-band magnitudes, and the grey crosses show LGS positions.

guide star signal level. Wavefront reconstruction involves a virtual DM formulation, and we use 12 virtual DMs, having found that there is insignificant performance gain when additional DMs (with associated increased simulation complexity) are introduced with the 35 layer atmosphere model. The reconstructed phase is then projected onto the physical DMs, which perform the AO correction. We model DMs using an interpolated spline function, which gives a good fit to surface models of most known DM types.

We assume an AO system update rate of 250 Hz, a baseline for MOSAIC, since the MOAO DMs will be operated in open-loop, and simulate 20 s of telescope time, verifying that the PSFs have converged. We note that the CANARY MOAO demonstration instrument (Myers et al. 2008) can also be operated at 250 Hz.

A previous study has shown that AO correction for the LGS configuration considered here is relatively constant over the field-of-view, differing by only a few percent in ensquared energy (Basden et al. 2013). Here, we therefore concentrate on the on-axis direction which is furthest from the LGS locations.

2.1.1 Guide star signal level

We base our NGS signal levels on r$'$ magnitudes, centred at $\lambda = 625$ nm with a $\delta\lambda = 140$ nm bandwidth (Fukugita et al. 1996). At magnitude 0, the r$'$ band gives a flux, F of 3631 Jy (Oke & Gunn 1983), and therefore a zero-magnitude star gives 1.23×10^{10} photons m^{-2} s^{-1}. We assume a telescope throughput of $T_{tel} = 90\%$ (see e.g., Puech et al. 2010), and a WFS throughput of $T_{wfs} = 85\%$, giving a final flux estimation equal to:

$$s = F \times J \times 10^{-0.4r'} \frac{A}{f} \times T_{tel} \times T_{wfs} \quad (1)$$

where s is the NGS signal in photons per sub-aperture per frame, and r' is the guide-star magnitude. $J = 1.51 \times 10^7$ photons per second per square metre per fractional bandwidth ($\frac{\delta\lambda}{\lambda}$). A is the sub-aperture area, 0.5^2 m^2, and f is the AO frame rate of 250 Hz.

Because there are many uncertainties in this flux calculation, we also investigate simulation performance as a function of a scaling of this signal level, allowing estimates to be updated once factors such as actual guide star observation band (and bandwidth, since WFSs can be very broadband with appropriate atmospheric dispersion correction) and detector quantum efficiency are known.

It should be noted that these signal levels are very faint. The faintest star in the NGS asterisms that we investigate has a r$'$ magnitude of 16.3, giving about 3 photons per sub-aperture per frame, according to Eq. 1. We take no special measures with such faint guide stars: they are processed in the same way as all others. However, because we use a maximum apriori wavefront reconstruction algorithm, WFS noise is taken into consideration, and signals from noisier wavefront sensors are penalised. Guide star signal levels could be increased by reducing the WFS frame rate. However, we do not consider this option here, partly because we are unable to easily operate LGS and NGS WFSs at different rates in our simulations, and because the improvement in performance would only be slight, for a large gain in complexity: we already take WFS noise into consideration in our wavefront reconstruction, and because the correction of the high spatial frequencies using high-order WFSs requires high time resolution, with reducing effectiveness as frame rate decreases. However, it should be noted that a reduction in NGS frame rate is likely to lead to a small improvement in AO performance when the faintest NGSs are considered.

We assume that LGS signal levels are not photon limited (Holzlöhner et al. 2010).

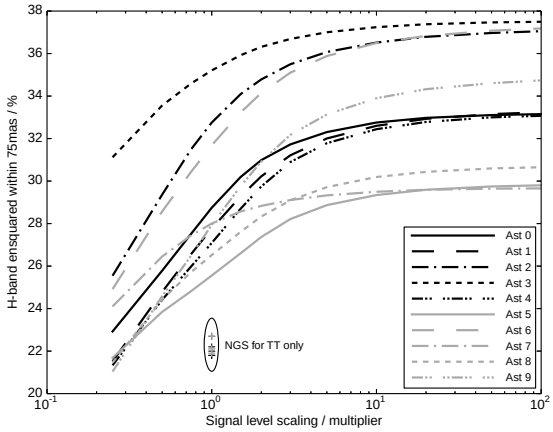

Figure 3. AO performance (ensquared energy) as a function of NGS asterism signal level scaling (with all guide star signals scaled by the X-axis value). For reference, the range of performance achieved when NGS information is used for tip-tilt correction only is also shown, and gives constant AO performance between signal level scales from one to 100. The legend provides the asterism number (ast).

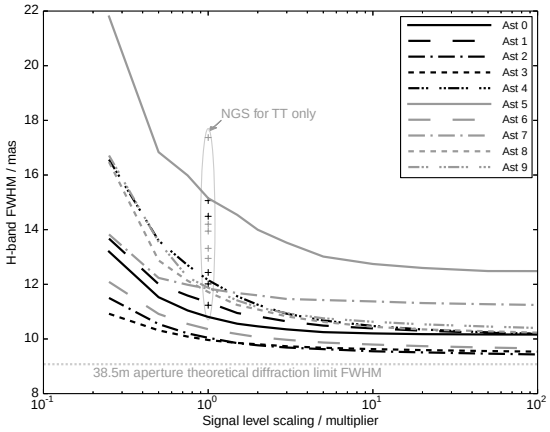

Figure 4. AO performance (FWHM) as a function of NGS asterism signal level scale (with all guide star signals scaled by the X-axis value). For reference, the range of performance achieved when NGS information is used for tip-tilt correction only is also shown, and gives constant AO performance between signal level scales from one to 100. The theoretical aperture limit is also shown, corresponding to the FWHM of a diffraction-limited spot on a 38.5 m aperture.

3 MOAO PERFORMANCE IN THE GOODS-S FIELD

Evaluating the AO performance for each asterism at the reference signal level alone will only give a performance snapshot for this signal level. We therefore consider increasing and reducing the signal levels across the board (i.e. for all NGS), for each asterism under consideration. Fig. 3 shows that the signal levels available for guide stars within the GOODS-S field are indeed low, and that an order of magnitude increase in flux (2.5 astronomical magnitudes) is required to ensure that there is then little performance gain by further increasing the signal levels. However, it also shows that at the reference flux levels, between 25-35% ensquared energy within 75 mas can be achieved (this increases to 30-38% when flux is not the limiting factor). The uncertainties within the model (based on repeat simulations) for this, and the following, figures are at the 1% level (not shown in the figures to aid clarity).

Fig. 4 shows the AO corrected PSF FWHM as a function of signal level, compared with the theoretical diffraction limit for a 38.5 m aperture. For the unmodified signal level (a scaling factor of unity), all asterisms lead to a PSF with a FWHM less than twice that of the theoretical, with some being only 10% larger. The PSFs themselves are shown in Fig. 5 for the case of default signal level. All the PSFs are well constrained, however, in the case of asterism 5, significant structure is displayed due to the presence of only two guide stars (one of which being very faint).

3.1 The effect of readout noise on AO performance

We have so far assumed that our detectors have no readout noise, with photon shot noise being the only WFS noise source. We now consider the AO performance when NGS readout noise is introduced. We have considered readout noise levels based on current detector technologies, ranging from 0.01 photo-electrons to 1 photo-electron. Fig. 6 shows the AO performance as a function of readout noise for the different NGS asterisms under consideration. Here we can see that noise can have a significant effect on performance, and therefore careful consideration should be given to the detector technology (EMCCD or sCMOS) used.

We have not considered detector quantum efficiency or the excess noise factor introduced by EMCCDs (which can effectively halve the quantum efficiency), though the effect that this has on performance can be garnered from Fig. 3: it can be seen that with a signal level scaling of 0.5 (due to the EMCCD excess noise factor), the AO performance is higher than that with a readout noise of 1 photo-electron in Fig. 6 (corresponding to an sCMOS detector). This suggests that EMCCD technology is more appropriate here.

Detector readout noise is key to the AO performance. However, our treatment of the effect of noise has been basic: we have simply removed a background level after adding readout noise (with a random Gaussian distribution) and relied on the minimum variance wavefront reconstruction. We have ignored sky background, which is low in the R′-band at 250 Hz frame rates. We have not considered more advanced techniques often employed in AO, for example pixel calibration based on brightest pixels within a sub-aperture (Basden et al. 2012), or Gaussian noise removal algorithms. The baseline for the EAGLE concept (Cuby et al. 2008), a forerunner for MOSAIC, was to use Shack-Hartmann wavefront sensors, and we have therefore not considered other sensor types. We have also not considered the benefits that could be obtained by reducing the number of NGS subapertures. Further, we have not considered the change in performance if the faintest stars within an asterism are disregarded (i.e. not used for AO), which may reduce noise propagation and hence increase AO performance. Therefore it is likely that performance improvements could be re-

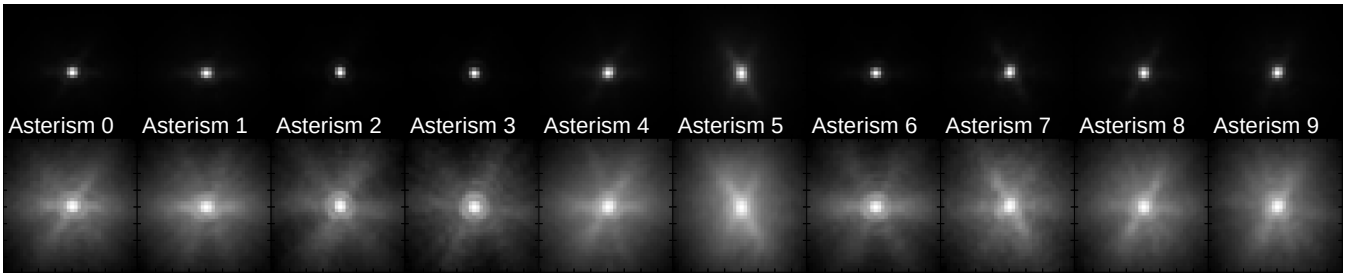

Figure 5. Simulated AO corrected H-band PSFs for the ten asterisms under consideration here. Each PSF box has an edge size of 177 mas. The top row shows the PSF, while the bottom row shows the natural logarithm of the PSF, showing the underlying hexagonal structure due to the LGS arrangement.

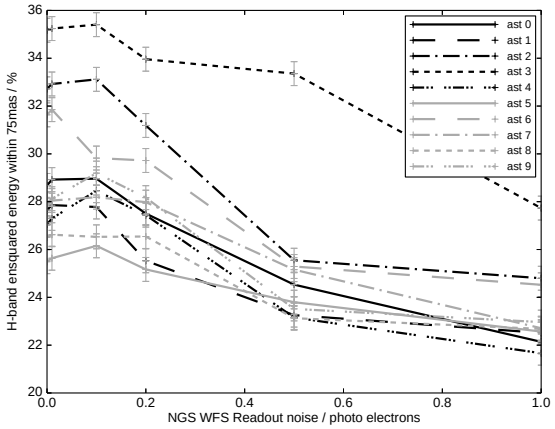

Figure 6. AO performance as a function of NGS readout noise, for the different asterisms under consideration here.

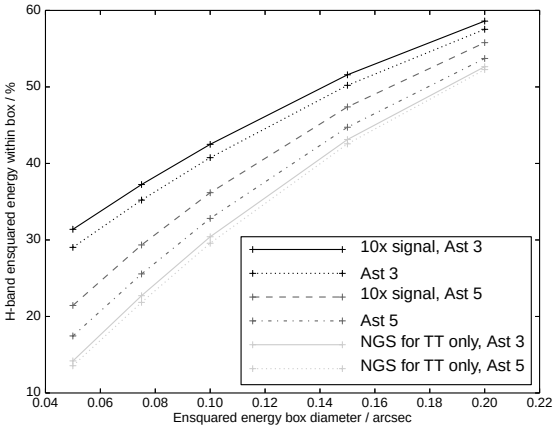
H-band ensquared energy within box / %
Ensquared energy box diameter / arcsec
10x signal, Ast 3
Ast 3
10x signal, Ast 5
Ast 5
NGS for TT only, Ast 3
NGS for TT only, Ast 5

Figure 7. The fraction of PSF energy ensquared as a function of box size. As shown in the legend, results are for the best (3) and worse (5) performing NGS asterisms, for three separate cases: when the NGS signal level is increased by a factor of ten, for the default NGS signal level, and for the case where NGS information is only used for tip-tilt correction.

alised when using noisy detectors over the results presented here, which can therefore be taken as pessimistic. The upper bound to performance, however, is given by the high flux cases in Fig. 3.

3.2 NGS for tip-tilt correction only

Given that the NGS signal levels are very low for many of the guide stars available within the selected GOODS-S sub-fields, it is worth considering the AO performance obtained when the NGS are used for tip-tilt correction only. Even using the faintest guide stars available provides ample signal for tip-tilt estimation, with thousands of photons collected across the telescope aperture. However, this then results in a lack of tomographic wavefront information, since the wide LGS asterism is unable to fully sample the turbulent volume. We find that the AO performance is reduced to about 22-23% ensquared energy within 75 mas, irrespective of the NGS asterism used (Fig. 3). NGS tip-tilt-only correction within the GOODS-S field is therefore not optimal: the high-order information obtainable from the NGSs is valuable. We also find that there is no increase in performance when guide star flux is increased by up to a factor of 100 beyond the nominal flux (levelling off at about 10 times flux, i.e. NGSs which are 2.5 magnitudes brighter than those studied here).

3.3 Ensquared energy diameter

The fractional ensquared energy as a function of spatial size on the sky is shown in Fig. 7. We have shown the best and worst asterisms in terms of performance (asterisms 5 and 7, respectively), and provide results for the default case, for an increase in the NGS signal by a factor of ten (where the AO performance approaches that of the high light-level case), and for when no high-order NGS information is used (i.e., the NGS are only used to determine the required tip-tilt correction). These results will directly inform design decisions for the MOSAIC concept, and their trends will be relevant to discussions of integral field unit (IFU) spaxel size verses expected performance for other future instruments.

We have selected our primary performance criterion to be the ensquared energy of the PSF within 75 mas, as motivated by the science simulations from Puech et al. (2008), with an updated discussion of these issues given by Evans et al. (2013). This spatial scale (sampled by two IFU spaxels) was the baseline for the EAGLE concept, and represents the most demanding requirement on spatial-resolution in recent studies of a MOAO-corrected MOS. As noted in §1, slightly coarser sampling of 100–150 mas (i.e. spatial pixels of 50-75 mas), with comparable ensquared energy, is suffi-

cient to recover the global properties of high-z galaxies. Such a spaxel size is also a good match for spectroscopic follow-up of resolved stellar populations observed with the *HST* and, in the future, the *JWST* (see discussion by Evans et al. 2013).

The top-level requirements for MOSAIC demand spaxel sizes which range from 40 to ∼100 mas (see Table 3 from Evans et al. 2014). Compared to the ensquared energy requirements from Puech et al. (2008), the 25–35% ensquared energy in 75 mas from the simulated fields in this work satisfy the most demanding requirements. Relaxing the spatial scales slightly (to, for example, the ensquared energy within 150 mas) leads to an ensquared energy estimate of 40–50% (Fig. 7). This would provide more than enough scope for additional reductions in performance from effects not modelled here (e.g., wavefront errors in the instrument could potentially degrade the ensquared energy by ∼10%, e.g., Laporte et al. (2010), while also satisfying the requirements for the vast majority of the science cases from Evans et al. (2013); Evans et al. (2014).

3.4 Future work

We have not considered techniques which make optimum use of NGS signals, rather relying on the minimum variance wavefront reconstruction with WFS noise covariance approximations. However, other approaches are also possible, which we intend to investigate. This includes the use of multi-rate WFSs, allowing lower frame rates for NGS observing faint targets, and a reduction of WFS order. Both techniques would increase the number of detected photons per sub-aperture per frame, and would therefore lead to more accurate wavefront slope estimation.

4 CONCLUSIONS

We have investigated the performance of an ELT MOAO instrument, giving consideration to the effect of NGS availability on performance. We have selected an existing deep cosmological field, the GOODS-S field, for this study, which is one of five fields observed as part of the *HST* CANDELS survey, providing rich scientific potential for ELT spectroscopy. Ten sub-fields within this region were chosen at random, and the expected AO performance investigated. Within each sub-field, we found at least two sufficiently bright NGSs, even though a key feature of the deep fields is that they are deliberately free of bright stars ($V < 14$). We have investigated the AO performance as a function of flux from these guide stars, to allow for uncertainties in detector efficiency and telescope optical throughput.

We find it is beneficial to use high-order wavefront information from faint natural guide stars as opposed to tip-tilt information. This conclusion should be revisited once the magnitude of additional tip-tilt components present within the system (e.g. from telescope vibrations) are better characterised.

Our key AO performance metric is the ensquared energy within 75 mas, which is between 25-35% for all of the NGS asterisms considered, reducing to about 22% when no high-order NGS information is used. An increase in ensquared energy to 40-50% is possible with a box size of 150 mas. The AO performance that we predict here is sufficient for the proposed MOSAIC instrument.

ACKNOWLEDGEMENTS

This work is funded by the UK Science and Technology Facilities Council, grant ST/K003569/1. This research has made use of the APASS database, located at the AAVSO web site. Funding for APASS has been provided by the Robert Martin Ayers Sciences Fund.

REFERENCES

Andersen D., Wang L., Ellerbroek B., Herriot G., 2011, in Second International Conference on Adaptive Optics for Extremely Large Telescopes. Predicted sky coverage for the TMT MCAO system NFIRAOS. p. 18P

Basden A., Myers R., Butterley T., 2010, Appl. Optics, 49, G1

Basden A. G., 2014, MNRAS, 440, 577

Basden A. G., Bharmal N. A., Myers R. M., Morris S. L., Morris T. J., 2013, MNRAS, 435, 992

Basden A. G., Butterley T., Myers R. M., Wilson R. W., 2007, Appl. Optics, 46, 1089

Basden A. G., Chemla F., Dipper N., Gendron E., Henry D., Morris T., Rousset G., Vidal F., 2014, MNRAS, 439, 968

Basden A. G., Haniff C. A., Mackay C. D., 2003, MNRAS, 345, 985

Basden A. G., Myers R. M., Gendron E., 2012, MNRAS, 419, 1628

Bournaud F., Elmegreen B. G., Elmegreen D. M., 2007, Ap.J., 670, 237

Calamida A., 2009, Technical Report E-TRE-ESO-080-0588, issue 1, stellar Counts for the E-ELT Sky Coverage Computations. European Southern Observatory

Cuby J.-G., Morris S., Bryson I., Lehnert M., Evans C., Fusco T., Jagourel P., Myers R., Rousset G., Schnetler H., 2008, in Ground-based and Airborne Instrumentation for Astronomy II. Edited by McLean, Ian S.; Casali, Mark M. Proceedings of the SPIE, Volume 7014, pp. 70141K-70141K-11 (2008). Vol. 7014 of Society of Photo-Optical Instrumentation Engineers (SPIE) Conference Series, EAGLE: an MOAO fed multi-IFU in the NIR on the E-ELT

Cuby J.-G., Morris S., Fusco T., Lehnert M., Parr-Burman P., Rousset G., Amans J.-P., Beard S., Bryson I., Cohen M., Dipper N., Evans C., Ferrari M., Gendron E., 2010, in Society of Photo-Optical Instrumentation Engineers (SPIE) Conference Series Vol. 7735 of Society of Photo-Optical Instrumentation Engineers (SPIE) Conference Series, EAGLE: a MOAO fed multi-IFU NIR workhorse for E-ELT

Evans C., Puech M., Barbuy B., Bastian N., Bonifacio P., Caffau E., Cuby J.-G., Dalton G., Davies B., Dunlop J., 2013, Technical report, ELT-MOS White Paper: Science Overview and Requirements. UK-ATC

Evans E., Puech M., Barbuy B., Bonifacio P., Cuby J., Guenther E., Hammer F., Jagourel P., Kaper L., Morris S., Afonso J. Amram P., Aussel H., Basden A., Bastian N.,

2014, in Society of Photo-Optical Instrumentation Engineers (SPIE) Conference Series Vol. in print of Society of Photo-Optical Instrumentation Engineers (SPIE) Conference Series, Science Case and Requirements for the MOSAIC Concept for a Multi-Object Spectrograph for the European Extremely Large Telescope

Fukugita M., Ichikawa T., Gunn J. E., Doi M., Shimasaku K., Schneider D. P., 1996, AJ, 111, 1748

Gardner J., Mather J., Clampin M., Doyon R., Greenhouse M., Hammel H., Hutchings J., Jakobsen P., Lilly S., Long K., Lunine J., Mccaughrean M., Mountain M., Nella J., Rieke G., Rieke M., Rix H.-W., Smith E., Sonneborn G., Stiavelli M., Stockman H., Windhorst R., Wright G., 2006, Space Science Reviews, 123, 485

Giavalisco M., Ferguson H. C., Koekemoer A. M., Dickinson M., Alexander D. M., Bauer F. E., Bergeron J., 2004, Ap.J.L., 600, L93

Glazebrook K., 2013, Pub. Ast. Soc. Australia, 30, 56

Grogin N. A., Kocevski D. D., Faber S. M., Ferguson H. C., Koekemoer A. M., Riess A. G., Acquaviva V., 2011, Ap.J.S., 197, 35

Hammer F., Barbuy B., Cuby J., Kaper L., Morris S., Evans C., Jagourel P., Puech M., 2014, in Society of Photo-Optical Instrumentation Engineers (SPIE) Conference Series Vol. in print of Society of Photo-Optical Instrumentation Engineers (SPIE) Conference Series, MOSAIC at E-ELT: a MOS for astrophysics, IGM, and cosmology

Holzlöhner R., Rochester S. M., Pfrommer T., Bonaccini Calia D., Budker D., Higbie J. M., Hackenberg W., 2010, in Society of Photo-Optical Instrumentation Engineers (SPIE) Conference Series Vol. 7736 of Society of Photo-Optical Instrumentation Engineers (SPIE) Conference Series, Laser guide star return flux simulations based on observed sodium density profiles

Laporte P., Schnetler H., Rousset G., 2010, in Society of Photo-Optical Instrumentation Engineers (SPIE) Conference Series Vol. 7738 of Society of Photo-Optical Instrumentation Engineers (SPIE) Conference Series, Integrating AO in a performance budget: toward a global system engineering vision

Marchetti E., Brast R., Delabre B., Donaldson R., Fedrigo E., Frank C., Hubin N., Kolb J., Lizon J.-L., Marchesi M., Oberti S., Reiss R., Santos J., CAMCAO Consortium 2007, The Messenger, 129, 8

Myers R. M., Hubert Z., Morris T. J., Gendron E., Dipper N. A., Kellerer A., Goodsell S. J., Rousset G., Younger E., Marteaud M., Basden A. G., 2008, in Society of Photo-Optical Instrumentation Engineers (SPIE) Conference Series Vol. 7015 of Presented at the Society of Photo-Optical Instrumentation Engineers (SPIE) Conference, CANARY: the on-sky NGS/LGS MOAO demonstrator for EAGLE

Newman S. F., Genzel R., Forster Schreiber N. M., Shapiro Griffin K., Mancini C., Lilly S. J., Renzini A., 2013, Ap.J., 767, 104

Oke J. B., Gunn J. E., 1983, Ap.J., 266, 713

Popesso P., Dickinson M., Nonino M., Vanzella E., Daddi E., Fosbury R. A. E., Kuntschner H., Mainieri V., Cristiani S., Cesarsky C., Giavalisco M., Renzini A., GOODS Team 2009, A&A, 494, 443

Puech M., Flores H., Lehnert M., Neichel B., Fusco T., Rosati P., Cuby J.-G., Rousset G., 2008, MNRAS, 390, 1089

Puech M., Rosati P., Toft S., Cimatti A., Neichel B., Fusco T., 2010, MNRAS, 402, 903

Spyromilio J., Comerón F., D'Odorico S., Kissler-Patig M., Gilmozzi R., 2008, The Messenger, 133, 2

Zacharias N., Finch C. T., Girard T. M., Henden A., Bartlett J. L., Monet D. G., Zacharias M. I., 2013, AJ, 145, 44

This paper has been typeset from a TEX/ LATEX file prepared by the author.

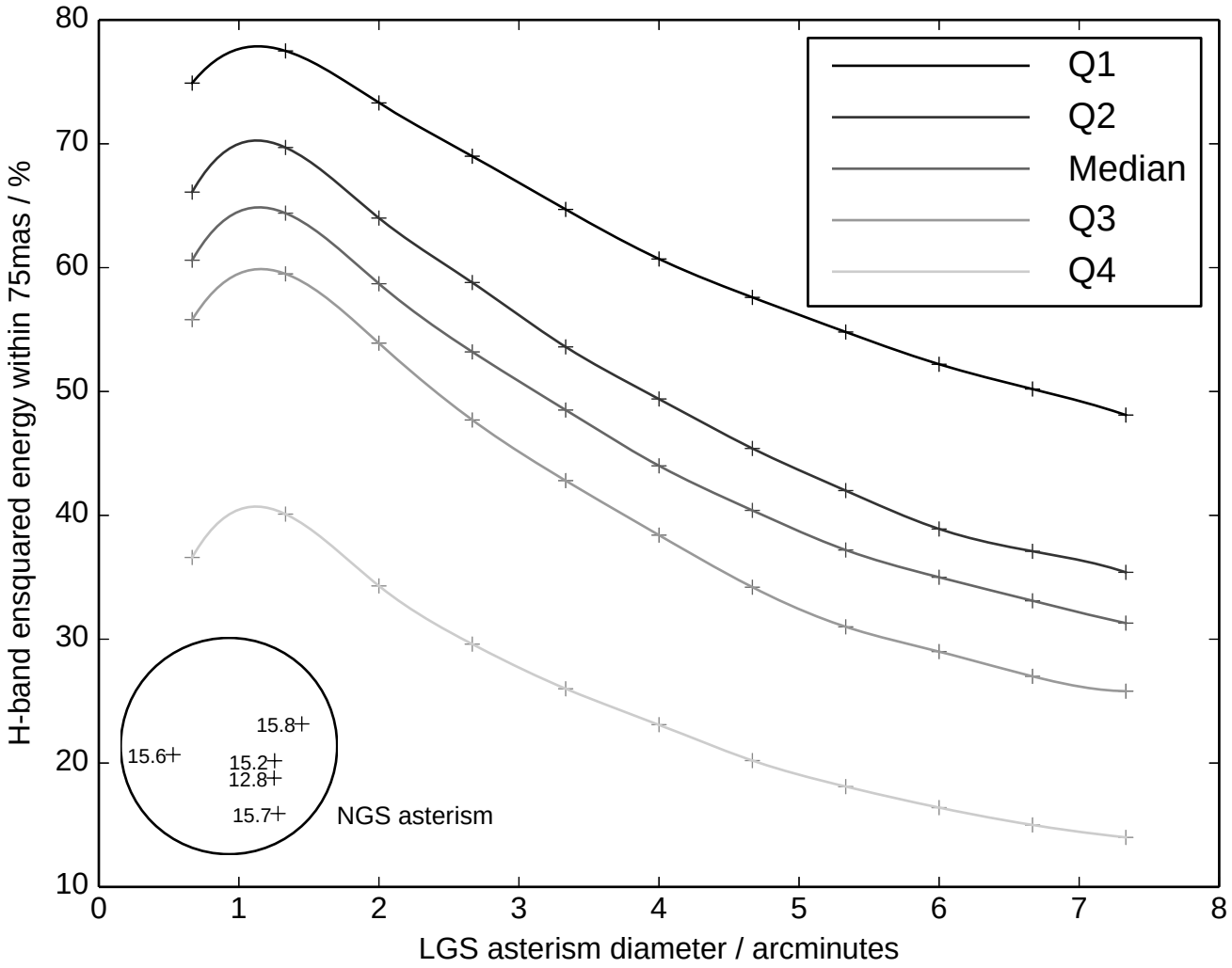
80
70
60
50
40
30
20
10
0
1
2
3
4
5
6
7
8
H-band ensquared energy within 75mas / %
LGS asterism diameter / arcminutes
Q1
Q2
Median
Q3
Q4
15.8
15.6
15.2
12.8
15.7
NGS asterism